SCA2003-16: A NUMERICAL STUDY OF THE INFLUENCE OF SAMPLE SHAPE ON SPONTANEOUS IMBIBITION

Douglas Ruth, University of Manitoba; Geoffrey Mason, Loughborough University; and Norman Morrow, University of Wyoming

This paper was prepared for presentation at the International Symposium of the Society of Core Analysts held in Pau, France, 21-24 September 2003

ABSTRACT

This paper reports on a numerical study of the effect of sample shape on spontaneous imbibition curves (recovery versus time) in a water-wet, laboratory scale system. Characteristic lengths based on the surface area open to imbibition and distance to the corresponding no-flow boundary, have been tested experimentally by Ma *et al.* for cylindrical samples with configurations having the following open surfaces: one-end, both-ends, the radial surface, and all surfaces. The present study addresses one-dimensional linear, and radially and spherically symmetric cases, and thus includes the first and third cases investigated by Ma *et al.* Also considered are annular-radial samples and hollow-spherical samples for a wide range of aspect ratio (inner radius divided by outer radius) with inner, outer, and both surfaces open. The numerical results show that, although the Ma *et al.* correlation is satisfactory within expected experimental error, annular and hollow spherical shapes, particularly for either the inner or outer face open, give systematic differences in shape of the spontaneous imbibition curves. Only minor differences in curve shape are obtained when both faces are open. The maximum differences occur for the smallest aspect ratio. The differences approach zero as the aspect ratio approaches one. An extension of the correlation, that weights the distance from the open surface with the local volume, gave close correlation of the simulated results for all cases. The results identify conditions under which differences in curve shape should be readily detectable by experiment.

INTRODUCTION

Numerical simulation studies can often both supplement and guide experimental work, thereby making the experimental programs more efficient. Furthermore, the ability to match experimental data provides confidence in using simulation to predict behavior for conditions that lie outside the range of experimental data used to develop empirical correlations. Whereas experiments for imbibition can take up to many months, numerical experiments can be run in a matter of minutes. By simulating experiments before they are run physically, test times can be evaluated, schedules for data collection can be developed, and physical configurations that may produce novel results can be evaluated. Numerical studies also allow mechanisms to be examined individually, thereby facilitating a fuller understanding of complex physical phenomena.

Morrow and Mason [1] have recently reviewed published work regarding displacement of oil by spontaneous imbibition of water. Several developments have been made in scaling of experimental data for spontaneous imbibition. Application of the scaling group originally proposed by Mattax and Kyte [2] is subject to highly restricted conditions essentially set out in the classic work on scaling by Rapoport [3]. Departure from one of these conditions, that the model and the prototype have similar geometry, is the main subject of the present paper.

Ma *et al.* [4] showed that a large body of spontaneous imbibition data for very strongly water-wet conditions could be correlated in the form of recovery expressed as a fraction of the final recovery versus dimensionless time. All of the imbibition data gave production curves of close to the same shape and they showed that these curves could be fitted with a form of Aronofsky [5] model. The best fit to all of the correlated data was given by (Viksund *et al.* [6])

$$\frac{R}{R_\infty} = 1 - \frac{1}{\left(1 + 0.04 t_D\right)^{1.5}} \tag{1}$$

where R is the recovery, $R_¥$ is the ultimate recovery, and

$$t_D = t \sqrt{\frac{k}{f}} \frac{s}{L_C^2 \sqrt{m_w m_o}}. \tag{2}$$

Here t is time, k is permeability, f is porosity, s is interfacial tension, m_w is the water viscosity, and m_o is the oil viscosity. L_C is a characteristic length that compensates for differences in sample size, shape, and the position of the open surface(s). Hereafter, $(L_C)^2$ will be referred to as the scale factor.

Ruth *et al.* [7] demonstrated that the basic shape of the imbibition curves could be simulated for linear systems using a conventional, finite-difference scheme. In the present paper, this scheme is extended to radial and spherical geometries, including annular-radial and hollow-spherical systems with open faces on either both or only one of the inner and the outer surfaces. The present work has two main objectives. The first is to identify conditions under which imbibition curve shape is significantly affected by sample shape and which faces are open. The second is to test the length scale correlation proposed by Ma *et al.* [4] for a wide range of geometries.

FORMULATION OF THE NUMERICAL SIMULATOR

The simulator, based on a conventional, explicit, finite-difference scheme, has been described in Ruth *et al.* [7]. A fundamental feature of the model is the definitions of transmissibilities at interfaces between grid-blocks. The modification to accommodate radial and spherical systems was simply to account for the specific coordinate system in

the definitions of these transmissibilities. In all cases, the grid-blocks were constructed such that, except for those on the face(s) of the sample, they had equal volumes. Grid blocks on the face(s) had zero volumes. All simulations reported in the present paper used 298 grid blocks. Additional grid blocks lead to only marginal differences in the simulated production curves. For any particular combination of sample shape and open face(s), identical results for the scaled production curves are ensured, regardless of sample size. Thus, the basic geometric condition derived by Rapoport [3] for scaling of two-phase flow is automatically satisfied by the computational scheme.

TEST PARAMETER SPECIFICATIONS

The present study used the same functions as those used previously by Ruth *et al.* [7]. The relative permeabilities were assumed as Corey [8] functions

$$k_{ro} = k_{roe}\left(\frac{S_o - S_{ro}}{1 - S_{ro}}\right)^{n_o} \tag{3}$$

and

$$k_{rw} = k_{rwe}\left(\frac{S_w}{1 - S_{ro}}\right)^{n_w} \tag{4}$$

Here S_w is the water saturation S_o is the oil saturation and 1-S_{ro} is the movable fraction of the oil. The initial water saturation is zero. This assumption was made to allow direct comparison with previous work. The endpoint relative permeabilities are denoted by k_{roe} and k_{rwe} while n_o and n_w are exponents that control the shapes of the curves. The capillary pressure (Pc) curve was assumed to be logarithmic in form, and related to the capillary pressure at which residual nonwetting phase is attained (Pc_t) by

$$Pc = Pc_t\left[1 - B\ln\left(\frac{S_w}{1 - S_{ro}}\right)\right] \tag{5}$$

where B is a scale parameter. The values of the test parameters are given in Table 1.

Table 1: The Test Parameters

Variable	Value	Units	Variable	Value	Units
f	0.215	-	k	600.0	mD
L	5.08	Cm	D	3.18	cm
m_o	1.00	Cp	m_w	1.00	cp
k_{roe}	1.0	-	k_{rwe}	0.04	-
N_o	1.756	-	n_w	2.018	-
S_{or}	0.43	-	S_{wi}	0.0	-
Pc_t	2.29	Kpa	B	5.255	-

The rock properties are typical of Berea sandstone. The length *(L)* is for all cylindrical cases and the diameter *(D)* is for the non-annular cylindrical cases. For spherical, annular-radial and hollow-spherical cases, sample dimensions were calculated so that the pore volumes of all samples were equal. Annular and hollow samples are characterized by an aspect ratio, *A*,

$$A = \frac{r_i}{r_o} \tag{6}$$

where r_i and r_o are the inner and outer radius respectively. Examples of cylindrical samples of different aspect ratio are shown in Plate 1. The aspect ratio is $\left(1/\sqrt{2}\right)$ at the transition where all inside radii of the annulus are greater than the radius of a solid cylinder. All hollow spheres lie outside the solid sphere when the aspect ratio is greater than $\left(1/\sqrt[3]{2}\right)$.

The simulations were run until 95% of the moveable non-wetting phase was produced. Data was output at equal increments of 5% of moveable non-wetting phase saturation. This allowed direct comparison among all cases. All cases involved counter-current, spontaneous imbibition without gravity effects.

COMPARISONS OF PRODUCTION CURVE SHAPES

The first step in analyzing the numerical results was to examine the shapes of the production curves. In order to do this, the linear case (the radial surface and one end closed) was used as the reference. All other cases were scaled. The scaling was achieved by calculating the average ratio of times for equal productions between any particular case and the linear case. When plotted, the scaled curves give a direct, visual comparison between the shapes of the production curves. For the chosen cylinder dimensions, imbibition rates for the sphere and for radial imbibition into the cylinder are respectively about 27 and 22 times faster than for the cylinder with one end open. From the scaled curves shown in Figure 1, at early times, recovery for the sphere is slightly faster than for the cylinder. The linear case is the slowest. At late times, the recovery times for the three geometries change to the opposite order with the radial (cylinder and sphere) results still showing only slight difference. The shapes of all of the production curves are essentially the same within expected experimental error.

Figure 2 shows results for annular-radial samples with only one face, either the inner or the outer, open. Again the linear case is used as the basis of comparison. For the cases of the outer surface open, the production curve shapes fall increasingly close to the linear case as the aspect ratio is increased. At the limit of a very thin annulus, the sample must act as a linear sample. Compared to the results for radial imbibition with the outer surface open, the shapes of the curves for the cases where the inner surface is open show greater deviation from the linear case. However, the results again approach the linear case for

high aspect ratio. The sequence in recovery versus time curves reverses and shows increasingly wide separation in recovery times for recoveries above about 33% of final oil recovery.

Figure 3 shows the results for the hollow-spherical samples. The trends are similar to those observed for the annular-radial cases; however, the separation at later recovery times for either outer surface or inner surface open are even greater for the spherical samples. Again, the behavior for both inner and outer surfaces open approaches the linear behavior as the aspect ratio approaches unity.

Results for both faces open, for both annular-radial and hollow-spherical samples, are presented in Figure 4. Remarkably, for these cases, the shapes of the curves are almost identical to that for the linear case. The combination of imbibition at the two surfaces results in a close approximation to imbibition into a linear sample.

ANALYSIS OF THE SCALE FACTOR OF Ma *et al*

Ma *et al.* [4] proposed a scale factor that for linear, and radially and spherically symmetric shapes reduces to

$$L_C^2 = \frac{V_B \quad L_S}{A_S} \tag{7}$$

Here V_B is the sample bulk volume, L_S is the distance from the no-flow boundary to the open face, and A_S is the area of the open face. The results for the cases of one face-open are given in the second column of Table 2.

In order to test the effectiveness of the scale factor, the values calculated from Eq. 7 (see Table 2) for various shapes were normalized with respect to the value calculated for the linear case. These normalized factors were cross-plotted against scale factors calculated by normalizing the simulated results for any shape with respect to the simulated results for the linear case (Figure 5). The line corresponds with 1-to-1 agreement. For both the radial and the spherical cases, the poorest agreement is for the zero aspect ratio and the outer surface open. As expected, the agreement improves as the aspect ratio increases. Agreement for the radial case is better than for the spherical case. The Ma *et al.* [4] correlation works very well for the cases of imbibition at the inner surface, except for the smallest aspect ratio, spherical case.

Table 2: Scale factors for cases with one face open.

Case	Ma *et al.* Correlation	New Correlation
Linear	L^2	$L^2/2$
Radial Outer Open	$\frac{\left(r_o^2 - r_i^2\right)\left(r_o - r_i\right)}{2r_o}$	$\frac{r_o^3/2 - r_o r_i^2/2 - r_o^3/3 + r_i^3/3}{r_o}$
Radial Inner Open	$\frac{\left(r_o^2 - r_i^2\right)\left(r_o - r_i\right)}{2r_i}$	$\frac{r_o^3/3 - r_i^3/3 - r_i r_o^2/2 + r_i^3/2}{r_i}$
Spherical Outer Open	$\frac{\left(r_o^3 - r_i^3\right)\left(r_o - r_i\right)}{3r_o^2}$	$\frac{r_o^4/3 - r_o r_i^3/3 - r_o^4/4 + r_i^4/4}{r_o^2}$
Spherical Inner Open	$\frac{\left(r_o^3 - r_i^3\right)\left(r_o - r_i\right)}{3r_i^2}$	$\frac{r_o^4/4 - r_i^4/4 - r_i r_o^3/3 + r_i^4/3}{r_i^2}$

A NEW CORRELATION

The Ma *et al.* [4] scale factor does not compensate for situations where incremental volumes of the sample do not have the same sizes at different distances from the open face. In order to account for this, the distance between any incremental volume and the open face can be weighted with the incremental volume and integrated over the entire volume. For the linear case the resulting equation for the scale factor is

$$L_C^2 = \frac{\int_0^L A\, x\, dx}{A} = \frac{L^2}{2} \tag{8}$$

For the radial case and the outer surface open, the result is

$$L_C^2 = \frac{\int_{r_i}^{r_o} 2p\, r\, L (r_o - r)\, dr}{2p\, r_o\, L} = \frac{r_o^3/2 - r_o r_i^2/2 - r_o^3/3 + r_i^3/3}{r_o} \tag{9}$$

For the radial case and the inner surface open, the result is

$$L_C^2 = \frac{\int_{r_i}^{r_o} 2p\, r\, L (r - r_i)\, dr}{2p\, r_i\, L} = \frac{r_o^3/3 - r_i^3/3 - r_i r_o^2/2 + r_i^3/2}{r_i} \tag{10}$$

The equations for the spherical cases are found in an analogous manner. The results for all the single face open cases are summarized in the third column of Table 2.

Comparisons between the new correlation and the simulated results are shown in Figure 6. The agreement, when compared with the Ma *et al.* [4] correlation, is improved for all except the inner surface open cases at the lowest aspect ratios. Overall agreement between the modified analytical scale factors and the simulated values is excellent.

For completeness, the normalized scale factors are given in Table 3.

FUTURE EXPERIMENTAL WORK

The present results suggest that all three basic sample shapes (a right cylinder in linear or radial flow and a solid sphere) will produce curves of roughly the same shape. Given variations in the properties of samples, it is doubtful if the indicated differences could be detected by experiment. For annular and hollow samples, there is a good possibility that differences could be detected, particularly if flow at the inner surface is tested for low aspect ratios. Annular-radial samples are of special interest because they can be readily fabricated for a wide range of aspect ratio. They also provide a useful representation of combined flow in a fractured porous media. Spherical samples are of more academic interest; they would be hard to fabricate, particularly in the hollow form. They were used here to test the limits of the correlations.

CONCLUSIONS

This paper provides a comprehensive set of numerical simulation results for one-dimensional, spontaneous imbibition into a water-wet porous media initially saturated by the nonwetting phase. The simulations show large differences in rate but only slight changes in shape between linear (a cylinder with one end open) and radial flow (a cylinder with two ends closed or a sphere, and annuli and hollow spheres with both faces open). The simulations predict significant systematic changes in imbibition-curve shape with sample shape for both annular and hollow spherical samples with one face open. Correlation of results was tested using an existing definition of characteristic length (scale factor) and a new definition that compensates for changes in sample volume with distance from the imbibition face for radial and spherical flow. The new definition provided very close correlation of the simulated results.

REFERENCES

1. Morrow, N.R. and Mason, G.: "Recovery of Oil by Spontaneous Imbibition", *Current Opinion in Colloid & Interface Science*, 6, p. 321-337, 2001.

2. Mattax, C.C. and Kyte, J.R.: "Imbibition Oil Recovery From Fractured, Waterdrive Reservoirs," *SPEJ*, June, p.177, 1962.

3. Rapoport, L.A.: “Scaling laws for use in design and operation of water-oil flow models”, *Trans. AIME,* 204, p. 143-150, 1955.

4. Ma, S., Morrow, N.R. and Zhang, X.: “Generalized Scaling of Spontaneous Imbibition Data for Strongly Water-Wet Systems”, *JPSE*, 18, p. 165-178, 1997.

5. Aronofsky, J.S., Masse, L. and Natanson, S.G.: “A Model for the Mechanism of Oil Recovery for the Porous Matrix Due to Water Invasion in Fractured Reservoirs,” *Trans. AIME,* 213, p.17, 1958.

6. Viksund, B.G., Morrow, N.R., Ma, S., Wang, W., and Graue, A.: “Initial Water Saturation and Oil Recovery From Chalk and Sandstone by Spontaneous Imbibition” Proceedings, 1998 International Symposium of Society of Core Analysts, The Hague, September 1998.

7. Ruth, D.W., Morrow, N.R., Li, Y. and Buckley, J.S.: “A Simulation Study of Spontaneous Imbibition”, *Proc. of the Int. Sym. of the SCA*, Abu Dhabi, UAE, Oct. 2000.

8. Corey, A.T: “The Interrelation Between Gas and Oil Relative Permeabilities”, *Producers Monthly*. p. 38-41, Nov 1954.

ACKNOWLEDGEMENTS

Support for this work was provided by the National Science and Engineering Research Council of Canada, British Petroleum/Amoco, Chevron, ELF/Total/Gas de France/IFP, JNOC, Phillips, Statoil, the Enhanced Oil Recovery Institute of the University of Wyoming, and the National Petroleum Technology Office of the U.S. Department of Energy.

Table 3: The values of the normalized scale factors calculated from simulation, the Ma *et al.* [4] correlation and the new correlation.

Case	Simulation	Ma *et al*	New
Linear	1.0000	1.0000	1.0000
Radial Outer Open: A=0.0	0.0461	0.0703	0.0469
Radial Outer Open:A=0.2	0.0434	0.0562	0.0437
Radial Outer Open:A=0.4	0.0362	0.0422	0.0362
Radial Outer Open:A=0.8	0.0136	0.0141	0.0135
Radial Inner Open:A=0.2	0.2720	0.2812	0.3437
Radial Inner Open:A=0.4	0.1116	0.1055	0.1205
Radial Inner Open:A=0.8	0.0181	0.0176	0.0182
Spherical Outer Open:A=0.0	0.0366	0.0744	0.0372
Spherical Outer Open:A=0.2	0.0359	0.0594	0.0364
Spherical Outer Open:A=0.4	0.0319	0.0437	0.0319
Spherical Outer Open:A=0.8	0.0109	0.0117	0.0109
Spherical Inner Open:A=0.2	1.1408	1.4842	2.0587
Spherical Inner Open:A=0.4	0.2878	0.2729	0.3464
Spherical Inner Open:A=0.8	0.0193	0.0183	0.0197

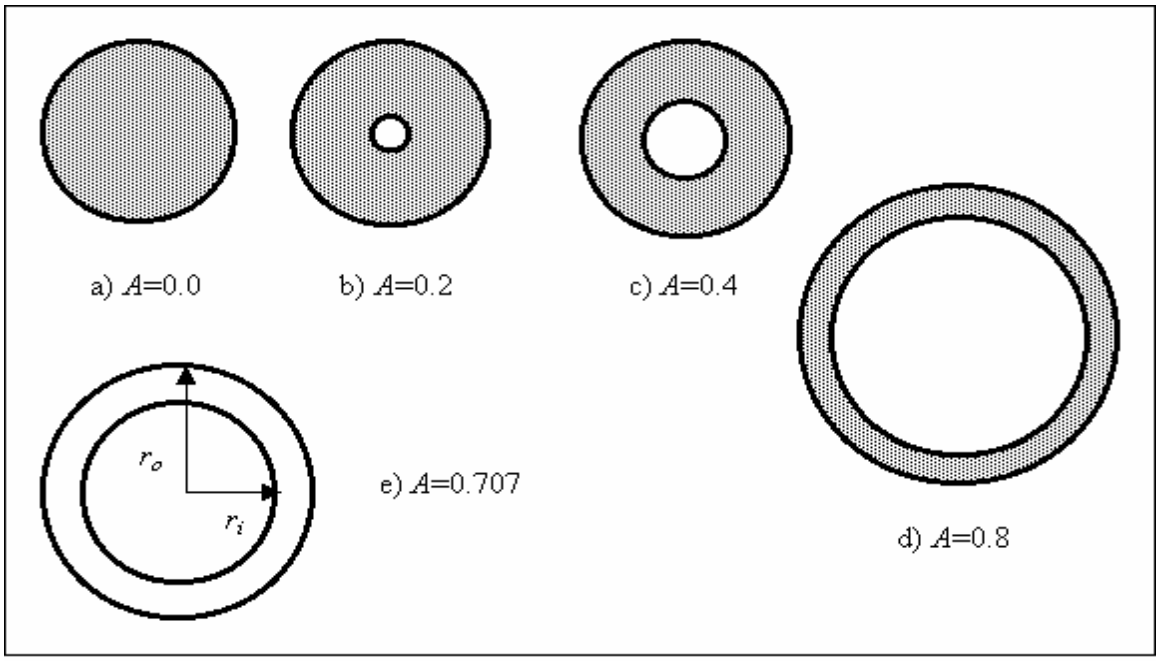

Plate 1: Examples of shapes of different aspect ratio given by annular samples. (Ratios of great circle diameters are used to define the aspect ratios of hollow spheres.). The first three have inner radii less than the radius of the solid cylinder; the fourth has an inner radius greater than the radius of the solid cylinder; the fifth example is the limiting case where the inner radius equals the radius of the solid cylinder. Cases a) to d) were studied in the present paper. Case e) is for illustrative purposes only.

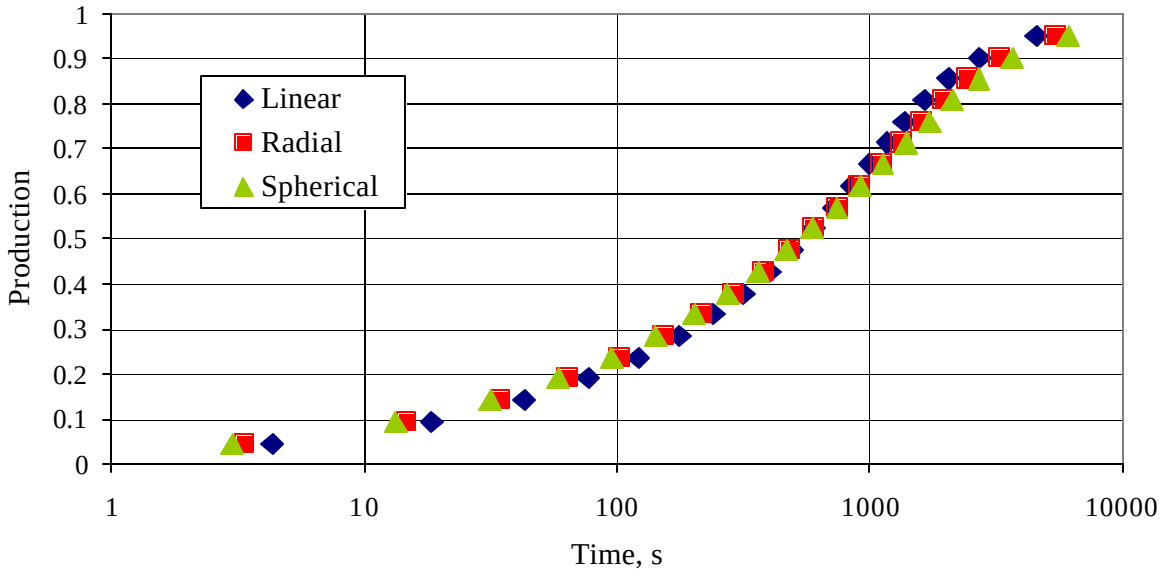

Figure 1: Normalized production as a fraction of mobile oil volume versus time. The radial and spherical cases have been linearly transposed to best match the linear case. Time is in seconds (times a linear best-fit scaling factor).

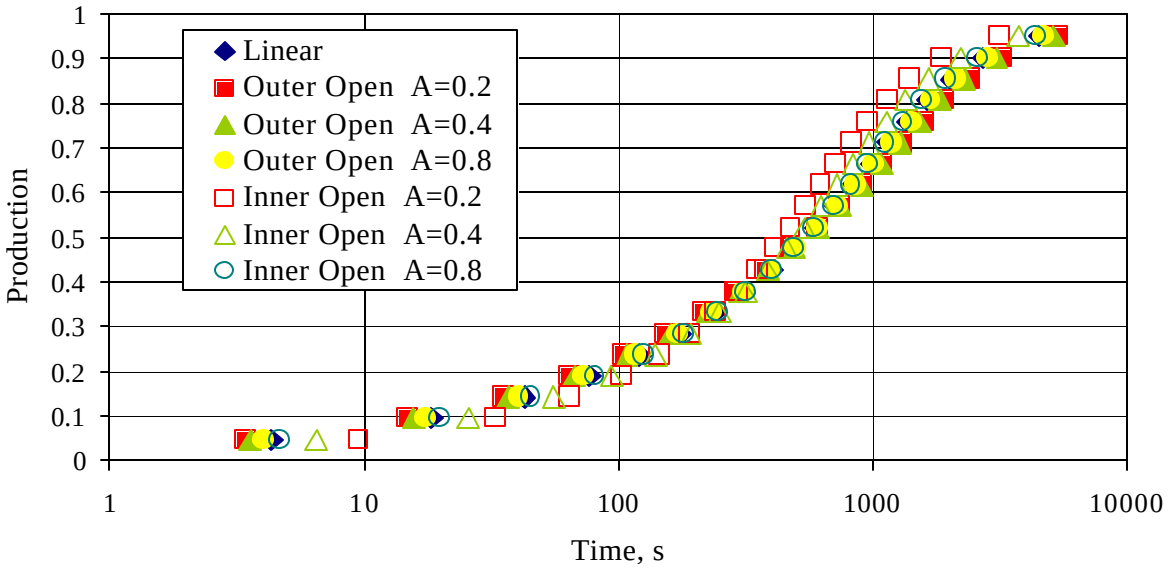

Figure 2: The radial cases for one surface open scaled to the linear case. Production is in fraction of mobile pore volume. Time is in seconds (times a linear best-fit scaling factor).

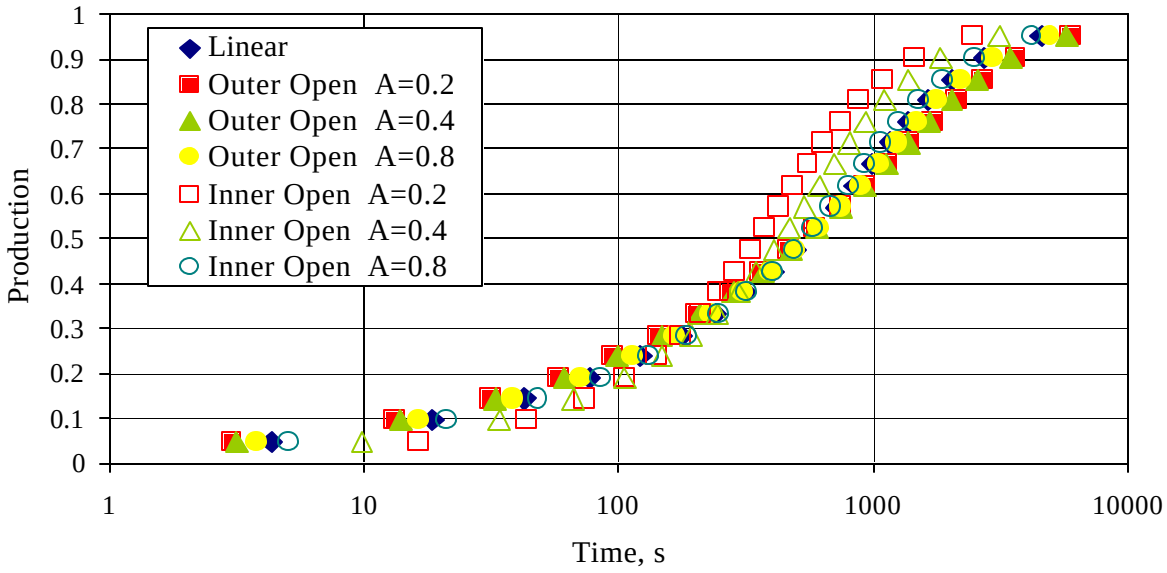

Figure 3: The spherical cases for one face open scaled to the linear case. Production is in fraction of mobile pore volume. Time is in seconds (times a linear best-fit scaling factor).

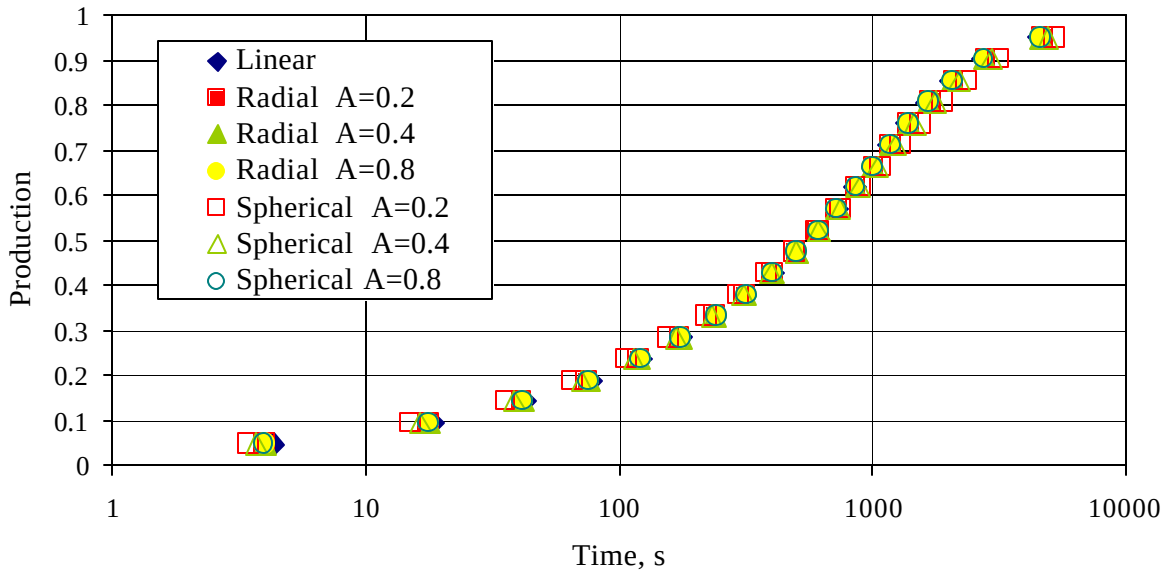

Figure 4: Production for cases where both inner and outer surfaces are open, scaled to the linear case. Production is in fraction of mobile pore volume. Time is in seconds (times a linear best-fit scaling factor).

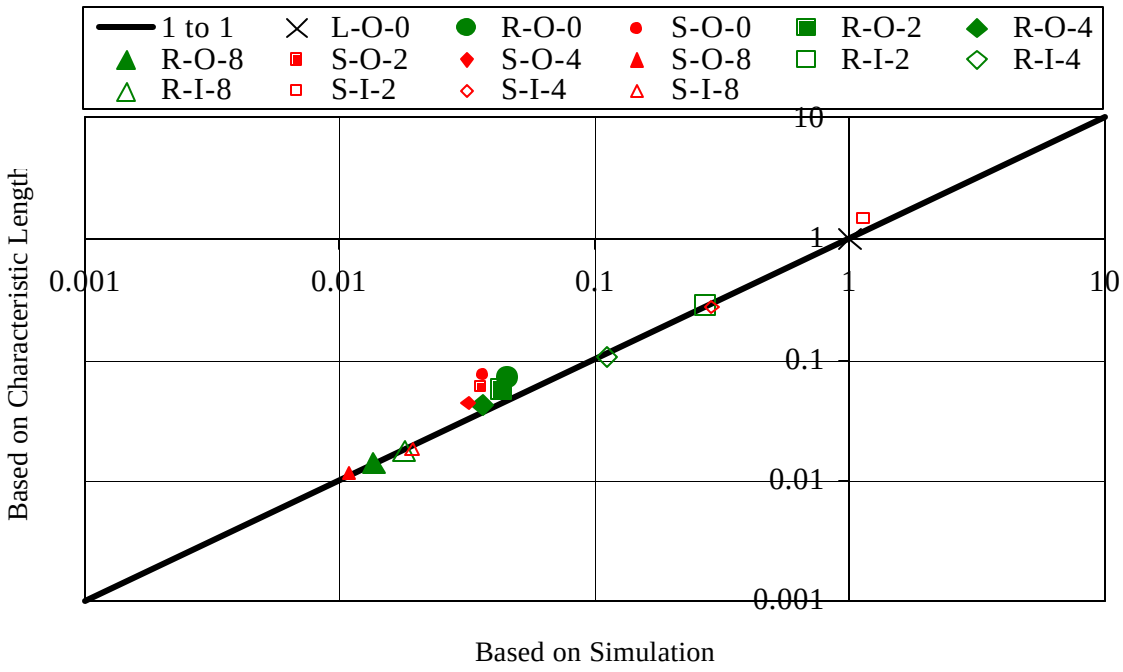

Figure 5: Correlation between the normalized scale factors predicted by the simulator and the values calculated by the Ma *et al.* correlation. L is linear; R is radial; S is spherical; O is outer face open; I is inner face open; 2,4,8 are aspect ratios in tenths.

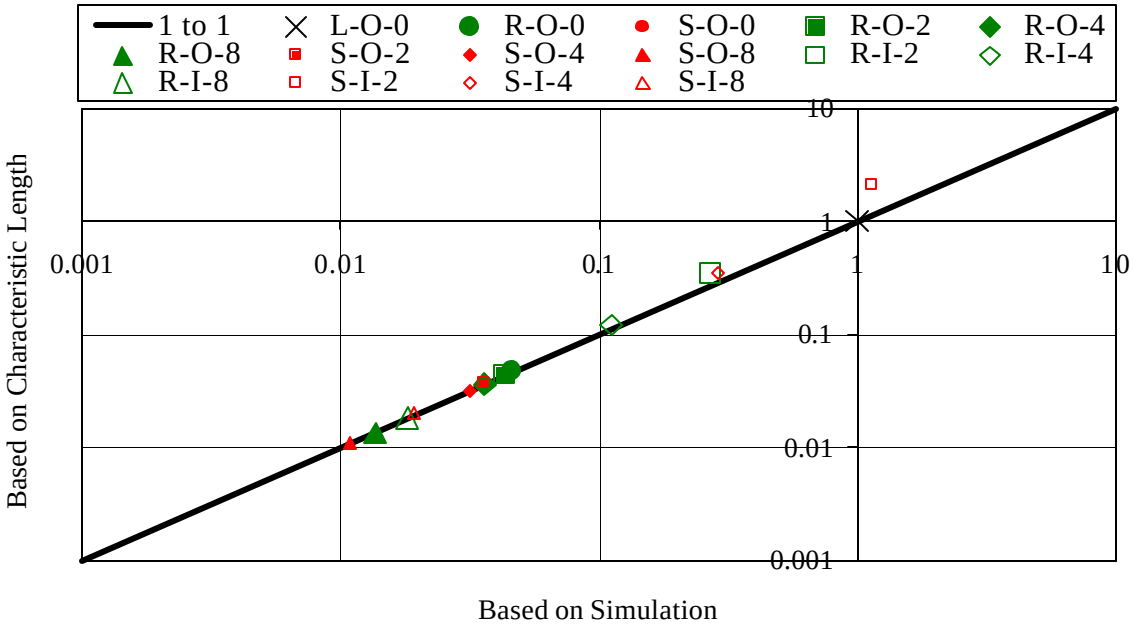

Figure 6: Correlation between the normalized scale factors predicted by the simulator and the values calculated by the improved correlation. L is linear; R is radial; S is spherical; O is outer face open; I is inner face open; 2,4,8 are aspect ratios in tenths.